Probing atomic and nuclear properties with precision spectroscopy of fine and hyperfine structures in the ^{7}Li^{+} ion

Hua Guan,[1,*] Shaolong Chen,[1,*] Xiao-Qiu Qi,[1,4] Shiyong Liang ,[1,4] Wei Sun,[1] Pengpeng Zhou,[1,4] Yao Huang,[1]
Pei-Pei Zhang ,[1,3,†] Zhen-Xiang Zhong ,[1] Zong-Chao Yan,[2,1,5] G. W. F. Drake ,[3] Ting-Yun Shi,[1,5] and Kelin Gao[1,5,‡]

[1]*State Key Laboratory of Magnetic Resonance and Atomic and Molecular Physics, Wuhan Institute of Physics and Mathematics,
Innovation Academy for Precision Measurement Science and Technology, Chinese Academy of Sciences, Wuhan 430071, China*
[2]*Department of Physics, University of New Brunswick, Fredericton, New Brunswick, Canada E3B 5A3*
[3]*Department of Physics, University of Windsor, Windsor, Ontario, Canada N9B 3P4*
[4]*University of Chinese Academy of Sciences, Beijing 100049, China*
[5]*Center for Cold Atom Physics, Chinese Academy of Sciences, Wuhan 430071, China*

Precision spectroscopy of Li^{+} is a promising testing ground for bound-state quantum electrodynamics (QED) and for measurements of nuclear properties such as the Zemach radius. We investigate the hyperfine and fine-structure splittings of the $2\,^{3}S_1$ and $2\,^{3}P_J$ states of ^{7}Li^{+} using saturated fluorescence spectroscopy based on a $\sim$460 eV metastable ion beam. We measure in particular the $2\,^{3}S_1$–$2\,^{3}P_J$ transitions in ^{7}Li^{+}. With a triple nested loop scanning method, the long-term drift and systematic uncertainties are reduced or eliminated, resulting in a total uncertainty of less than 100 kHz. Our results are in good agreement with QED calculations. For the hyperfine splittings of $2\,^{3}S_1$, our measured values have a similar accuracy to previous measurements and theoretical calculations. For the $2\,^{3}P_J$ fine and hyperfine splittings, our measured results are one order of magnitude more accurate than those of previous measurements and have a similar accuracy to the theoretical values. The measurements lay the foundation for future work on the Li^{+} isotopes and their theoretical interpretation in terms of nuclear charge radii and the Zemach radii.

Two-electron atomic systems provide a key testing ground for quantum electrodynamics (QED) in systems more complicated than hydrogen. Helium has been the main focus for past works, both theoretically and experimentally [1–9]. On the theoretical side, the nonrelativistic eigenvalue problem can be solved variationally to very high precision. Relativistic and QED effects can then be taken into account perturbatively. Experimentally, the $2\,^{3}P_J$ fine structure of helium has larger fine-structure splittings and longer lifetimes than hydrogen, and some transition wavelengths are in a region suitable for precision laser spectroscopy. With QED corrections up to order $m\alpha^7$ included, the current theoretical prediction for the helium $2\,^{3}P_J$ fine structure reaches an accuracy of 1.7 kHz [3]. The excellent agreement between theory [3] and experiment [4] provides one of the best tests of bound-state QED in a multielectronic system. It also opens a window for an independent determination of the fine-structure constant α with an accuracy of 2 ppb, once the theory at the next order $m\alpha^8$ is complete.

The present Rapid Communication extends high-precision measurements to the heliumlike ion Li^{+}. There are two primary motivations for this. First, since the leading QED correction increases in proportion to Z^4, where Z is the nuclear charge, it is about one order of magnitude larger than

in hydrogen or helium. Second, since the next higher-order QED corrections increase in proportion to Z^6, it is possible to disentangle the different contributions as a function of Z. In addition, since lithium has several isotopes (including the ^{11}Li halo nucleus), measurements on different isotopes can be used to extract information on relative nuclear charge radii [10,11], and especially the Zemach radius from the hyperfine structure and the magnetic moment distribution inside the nucleus. The results provide valuable tests of nuclear structure models [10,12].

The spectroscopy of Li^{+} has been investigated experimentally for nearly a century [13]. Various methods have been introduced to measure hyperfine and fine-structure intervals of $2\,^{3}P_J$ and $2\,^{3}S_1$ states in ^{7}Li^{+}, such as the beam-foil technique [14], Doppler-tuned spectroscopy [15], laser-microwave spectroscopy [16,17], and saturated spectroscopy [18,19]. The most recent measurement was performed using the electro-optic modulator (EOM) modulation spectroscopy by van Wijngaarden's group [20,21], using nearly collinear laser and ion beams. Because of the Doppler effect, the asymmetric spectral profile, and the unstable ion source [22], the uncertainties in their fine and hyperfine structures of $2\,^{3}P_J$ reach several hundreds of kHz [20]. Up to now, for the hyperfine-structure intervals of $2\,^{3}S_1$, the most accurate measurement is from the laser-microwave spectroscopy of Kötz *et al.* [16], where the uncertainty is 40 kHz. For the $2\,^{3}P_J$ fine- and hyperfine-structure intervals, the most accurate measurements are from the laser-microwave spectroscopy of Kowalski *et al.*

---

*These authors contributed equally to this work.
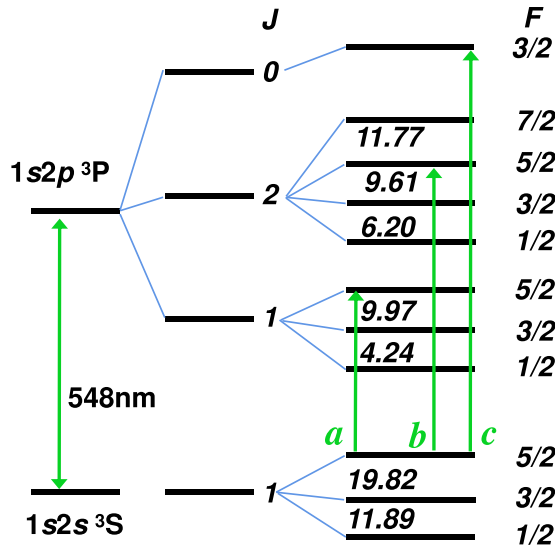†zhangpei@wipm.ac.cn
‡klgao@wipm.ac.cn

FIG. 1. Energy levels of $2\,^3S_1$ and $2\,^3P_J$ states of $^7\mathrm{Li}^+$ (not to scale). Units are in GHz. The transitions labeled by *a*, *b*, and *c* are used to determine the fine-structure splittings of $2\,^3P_J$.

[17] and from the EOM modulation spectroscopy of Clarke *et al.* [20], where the uncertainties are a few hundred kHz.

In this Rapid Communication, we report measurements of the fine and hyperfine structures for the $2\,^3P_J$ and $2\,^3S_1$ states of $^7\mathrm{Li}^+$ using saturated spectroscopy based on a collimated ion beam of $\sim$460 eV energy. Using the Lamb dip signal with the Doppler background subtracted, we determine the central frequency of each spectral line by fitting the Lamb dip signal with the data from more than 250 h of continuous measurement. We achieve a measurement accuracy at the level of a few tens of kHz.

A partial energy-level diagram of $^7\mathrm{Li}^+$ is shown in Fig. 1. In our experiment, the measurement scheme is as follows. To measure the hyperfine splittings of the $2\,^3P_J$ state, we choose a certain lower substate in $2\,^3S_1$ and probe transitions to different hyperfine levels of $2\,^3P_J$ with fixed *J*. To measure the hyperfine splittings of the $2\,^3S_1$ state, we fix a hyperfine level in $2\,^3P_2$ and probe the transitions from different hyperfine levels of $2\,^3S_1$. To measure the fine-structure intervals of $2\,^3P_J$, we probe the transitions (see *a*, *b*, *c* in Fig. 1) from a fixed lower state in $2\,^3S_1$ to different upper states (J, F) of $2\,^3P_J$. Combining our measurements and previous theoretical results of hyperfine shifts [11], we can determine the fine-structure splittings of the $2\,^3P_J$ state.

Our apparatus setup is shown in Fig. 2, which has been detailed in our previous work [23,24]. In brief, the whole device is composed of an ion source, laser system, and fluorescence detector. Li^+ ions (more than 90% of the composition is $^7\mathrm{Li}^+$) are generated by the electron beam bombarding the atomic beam. The 548-nm laser is generated by the second-harmonic generation of a 1097-nm narrow-band fiber laser (Y10, NKT Photonics), which is stabilized to a wave meter (WS-7, HighFinesse). The 548-nm laser frequency is measured by a femtosecond optical comb (FC8004, Menlo Systems) referenced to a hydrogen clock (CHI-75A, Kvarz). A photomultiplier tube (PMT, 9893, ET Enterprises) is adopted to detect fluorescence.
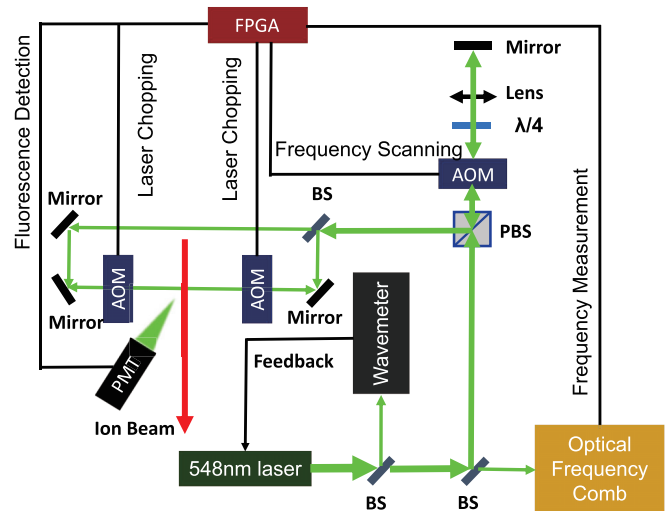

FIG. 2. The apparatus for the spectroscopy measurement of $^7\mathrm{Li}^+$. The green lines represent optical paths and the dark lines represent electronic connections. For details, see the text. AOM: acoustic optical modulator; BS: beam splitter; PBS: polarized beam splitter; $\lambda/4$: $\lambda/4$ wave plate; PMT: photomultiplier tube; FPGA: field-programmable gate array.

Here, two 548-nm laser beams of the same frequency are reversely overlapped and interact with the ion beam at right angles. By using three acoustic optical modulators (AOMs) for laser chopping and frequency scanning, a triple nested loop scan method [23] is adopted to obtain the Lamb dip signal without background and to measure the frequency gap between two different transitions. This method can greatly reduce the influence of the system's long-term drift. Figure 3 shows the hyperfine splitting between $F = 1/2$ and $F = 3/2$ of $2\,^3P_2$, where the full width at half maximum (FWHM) of the Lamb dip signal is about 50 MHz. The determined hyperfine splitting is 6203.319 MHz, with the statistical uncertainty being 61 kHz.

For the $2\,^3P_J$ fine-structure intervals, because of the existence of a hyperfine structure, we determine the fine splittings by combining the special hyperfine transitions of different *J* in $2\,^3P_J$ with the theoretical results of Drake *et al.* [11]. For measuring the $2\,^3P_1 - 2\,^3P_0$ splitting, for example, we probe two transitions of $2\,^3S_1, F = 5/2 \leftrightarrow 2\,^3P_1, F = 5/2$ and $2\,^3S_1, F = 5/2 \leftrightarrow 2\,^3P_0, F = 3/2$. As seen from Fig. 4, the central value of the difference between these two transitions is 15 2075.428(65) MHz. Combining our measurements and the previous theoretical results of hyperfine shifts [11], together with the 11 kHz second-order Doppler shift correction, we can derive the fine-structure splitting between $2\,^3P_1$ and $2\,^3P_0$ according to $15\,2075.428(65) + 4442.03 - 812.97 + 0.011 = 15\,5704.499(65)$ MHz.

In total, all hyperfine splittings of $2\,^3S_1$ and $2\,^3P_J$ as well as the fine-structure splittings of $2\,^3P_J$ are measured. Various systematic effects have been considered, as analyzed below.

Doppler effect. The motion of ions and imperfect overlap of the two lasers introduces a Doppler shift. We monitor the misalignment of the two lasers by the Lamb dip center [25], which is found to be below 25 μrad. The misalignment causes a first-order Doppler shift of 5 MHz to each peak. Since
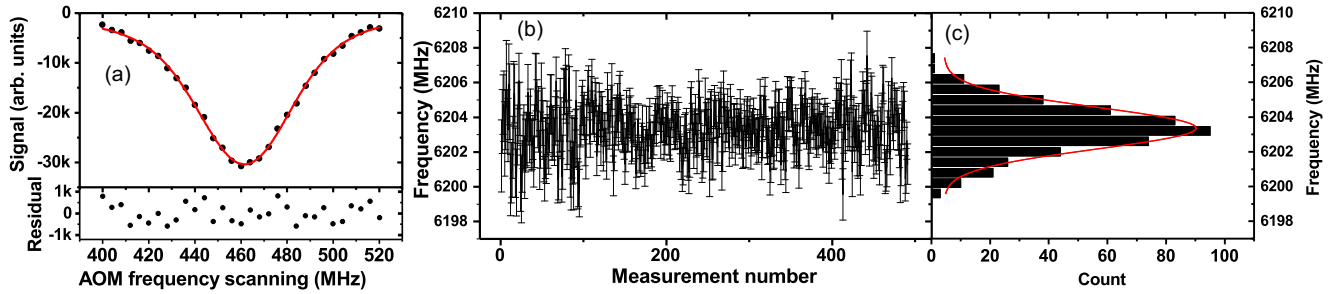
FIG. 3. Measurement of the hyperfine splitting between $F = 1/2$ and $F = 3/2$ of the $2\,^3P_2$ state. (a) Pure Lamb dip signal of a transition with a Voigt plus Fano fitting curve. (b) The statistical distribution of the measurement. (c) The histogram of the measurement.

we measure the difference between two peaks, the shifts are almost canceled and thus the uncertainties of first-order and second-order Doppler shifts are estimated to be below a few kHz.

Laser power. According to the theoretical analysis by Artoni *et al.* [26], the laser power introduces a shift in the Lamb dip signal, which is related to interaction time, while in our experiment, the interaction time between the ions and lasers is only 22 ns. Comparing with previous experiments of He [6] and Li$^+$ [25], the shift caused by laser power should be very small in our experiment. We measure the $2\,^3P_2$ hyperfine splitting between $F = 3/2$ and $F = 5/2$ at different laser powers and find that there is no detectable shift. We assign an upper limit on the uncertainty to be 11 kHz.

Laser frequency measurement. We measure the 548-nm laser frequency by a fs comb referenced to a hydrogen maser. Since the stability of the H maser is better than 1×10^{-11}, we estimate that the upper limit on the uncertainty due to the frequency measurement is 5 kHz.

Zeeman effect. Since the residual magnetic field in our experiments is about 0.39 G and the purity of linear polarization of the lasers is higher than 99%, we can estimate a 1% first-order Zeeman shift to the Lamb dip signal. We calculate the first- and second-order Zeeman shifts to the splittings to be a few kHz and below 1 kHz, respectively.

Quantum interference. In our experiment, the profile of the Lamb dip signal is not always perfectly symmetric due to the quantum interference, asymmetric velocity distribution of the ion beam, and variable laser power intensities. To each transition, the effects from velocity distribution and variable

laser power are approximately equal and can thus be canceled in our splitting measurements. To estimate the effect of quantum interference, we use a Fano-Voigt line shape to do profile fitting, which has been proven to be effective in eliminating the quantum interference [27]. We assign an upper limit of 100% uncertainty to our estimated shift.

Other systematic effects, such as the dc Stark effect and collisional effect, have also been considered. For the dc Stark effect, it can be neglected since the electric field caused by the space-charge distribution is only 4 V/m. The collisional effect is also negligible since the vacuum pressure is lower than 2×10^{-6} Pa.

As an example, the uncertainty budget for the hyperfine splitting between $F = 3/2$ and $F = 5/2$ of the $2\,^3P_2$ state is given in Table I. The statistical uncertainty is estimated to be 44 kHz in 1σ and the total systematic uncertainty is 30 kHz. With these, we obtain this hyperfine splitting to be 9608220 ± 53 kHz.

Having taken into account the statistical and all the systematic uncertainties, we have obtained all the hyperfine splittings of $2\,^3P_J$ and $2\,^3S_1$, as shown in Table II. The $2\,^3P_J$ fine-structure splittings are listed in Table III. Our values of the hyperfine splittings of $2\,^3P_J$ have improved the previous experimental results by about one order of magnitude and most of the splittings have uncertainties below 100 kHz. The recent measurements by Clarke and van Wijngaarden [20] and by Kowalski *et al.* [17] have uncertainties over 500 kHz and they do not agree well with each other for some intervals, such as the $F = 5/2$–$F = 7/2$ interval in $2\,^3P_2$. Our results, on the other hand, agree with most of the previous values including
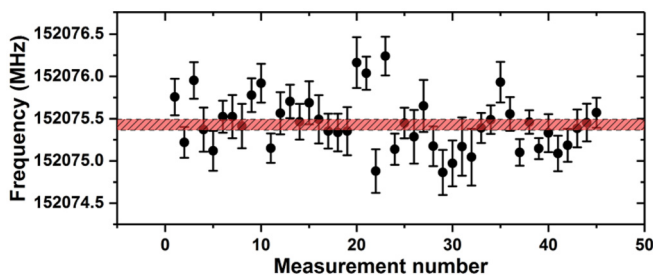

FIG. 4. Measurement of the splitting between $(2\,^3P_0, F = 3/2)$ and $(2\,^3P_1, F = 5/2)$. The average value is 152075.428 MHz with a statistical uncertainty of 65 kHz.

TABLE I. Uncertainty budget for the hyperfine splitting between $F = 3/2$ and $F = 5/2$ in $2\,^3P_2$, in kHz.

Source	ν	$\Delta\nu$
Statistical	9608220	44
First-order Doppler effect		< 1
Second-order Doppler effect		< 1
Laser power		11
Laser frequency measurement		5
Zeeman effect		1
Quantum interference		27
Total	9608220	53

TABLE II. Experimental and theoretical hyperfine transition frequencies in $2\,^3P_J$ and $2\,^3S_1$, in MHz, with $C_{\text{nuc\&ho}} = -0.057(1)$ and $Q_d = -0.0400(3) \times 10^{-24}$ cm^2 [28].

State	(J, F)–(J', F')	Experiment			Theory	
		Refs. [16,17]	Clarke *et al.* [20]	This work	Riis *et al.* [11]	This work
$2\,^3P_2$	$(2, 1/2)$–$(2, 3/2)$	6203.6(5)	6204.52(80)	$6203.319 \pm 0.061(\text{stat.}) \pm 0.026(\text{syst.})$	6203.27(30)	6203.391(145)
	$(2, 3/2)$–$(2, 5/2)$	9608.7(20)	9608.90(49)	$9608.220 \pm 0.044(\text{stat.}) \pm 0.030(\text{syst.})$	9608.12(15)	9608.277(83)
	$(2, 5/2)$–$(2, 7/2)$	11775.8(5)	11774.04(94)	$11772.965 \pm 0.029(\text{stat.}) \pm 0.068(\text{syst.})$	11773.05(18)	11772.957(84)
$2\,^3P_1$	$(1, 1/2)$–$(1, 3/2)$	4237.8(10)	4239.11(54)	$4238.823 \pm 0.081(\text{stat.}) \pm 0.075(\text{syst.})$	4238.86(20)	4238.776(75)
	$(1, 3/2)$–$(1, 5/2)$	9965.2(6)	9966.30(69)	$9966.655 \pm 0.054(\text{stat.}) \pm 0.086(\text{syst.})$	9966.14(13)	9966.331(52)
$2\,^3S_1$	$(1, 1/2)$–$(1, 3/2)$	11890.018(40)	11891.22(60)	$11890.088 \pm 0.063(\text{stat.}) \pm 0.012(\text{syst.})$	11890.013(38)	
	$(1, 3/2)$–$(1, 5/2)$	19817.673(40)	19817.90(73)	$19817.696 \pm 0.040(\text{stat.}) \pm 0.012(\text{syst.})$	19817.680(25)	

experimental and theoretical results, providing an independent check on those measurements. However, for $F = 5/2$–$F = 7/2$ in $2\,^3P_2$, our result barely agrees with the one of Clarke and van Wijngaarden [20], and has a 5σ discrepancy with the Kowalski *et al.* [17] value. Besides, for the hyperfine splitting $F = 3/2$–$F = 5/2$ in $2\,^3P_1$, the previous theoretical result 9966.14(13) [11] differs from our result by 515 kHz (4σ). We hope that these discrepancies can be resolved by more independent measurements and calculations. As for $2\,^3S_1$, our laser spectroscopy measurements agree well with the results obtained by the laser-microwave method [16,17] and about one order of magnitude better than the results of Clarke and van Wijngaarden [20]. For the $2\,^3P_J$ fine-structure splittings, our results are about 1.1 ppm for the $2\,^3P_1$–$2\,^3P_2$ interval and 0.7 ppm for the $2\,^3P_1$–$2\,^3P_0$ interval, which is an order of magnitude better than the results of Clarke and van Wijngaarden [20,22]. In comparison with theory, after subtracting the lower-order terms, the contribution from terms of order $m\alpha^6$ and higher for the $2\,^3P_1$–$2\,^3P_2$ interval is $-170.74(7)$ MHz, in agreement with the theoretical value $-170.67(5)$ MHz [3]. The magnitude is a factor of 26 larger than for helium, and verifies the high Z dependence.

For the QED theory of fine and hyperfine structure, we follow the method as applied to ^{3}He [2]. The details, however, are not exactly the same since the spin of the ^{7}Li$^+$ nucleus is 3/2 and not 1/2. We calculate the relativistic corrections of orders $m\alpha^4$ and $m\alpha^6$, and the QED corrections of order $m\alpha^6$. The contribution from the nuclear electric quadrupole moment is also taken into account. It is very important to estimate the contribution from the nuclear structure since the hyperfine structure is mainly induced by the interaction between the magnetic dipole moment of the nucleus and the electrons. We adopt the same method used in Ref. [2] to consider the nuclear effect. Since high-precision experimental measurements for the ground state of Li^{2+} are not available to

our knowledge, we use the precisely measured results for the hyperfine structure of the Li$^+$ $2\,^3S_1$ state instead [16,17]. By combining our calculations of the hyperfine structure with the precision measurement for the $2\,^3S_1$ state, we have derived the coefficient of the nuclear-structure and higher-order QED contributions $C_{\text{nuc\&ho}} = -0.057(1)$, defined in Ref. [2]. Since we have calculated the order $m\alpha^6$ correction, the next higher-order contribution to $C_{\text{nuc\&ho}}$ is $m\alpha^7$, which is completely negligible at the present level of experimental accuracy. Thus, the nuclear part of $C_{\text{nuc\&ho}}$ can be extracted that is independent of the electronic state of interest. We can apply the thus determined nuclear term to calculations of the hyperfine structure of $2\,^3P_J$. The final theoretical results for the $2\,^3P_J$ hyperfine structure are listed in Table II, together with a comparison with experimental values. Full details of the QED calculations will be published separately [29].

The present theoretical results agree with previous calculations of Drake in Ref. [11] but have one more significant digit due to the inclusion of order $m\alpha^6$ corrections. The only discrepancy between Drake and the present calculation for the $F = 3/2$–$F = 5/2$ in the $2\,^3P_1$ interval is due to the use of a different value for the nuclear electric quadrupole moment. We attribute the dominant uncertainty in our calculated hyperfine structure to the nuclear effect. A more accurate $C_{\text{nuc\&ho}}$ could be determined if a further improvement can be achieved for the measurement of the $2\,^3S_1$ hyperfine structure. Similarly, a more precise value for the Zemach radius could also be extracted from the coefficient $C_{\text{nuc\&ho}}$. Our calculations are in good agreement with the present measurements except for the interval $F = 3/2$–$F = 5/2$ of $2\,^3P_1$, for which we do not have a satisfactory explanation. The present work lays the foundation for future spectroscopic measurements on the Li$^+$ isotopes and their theoretical interpretation in terms of nuclear charge radii and the Zemach radii.

TABLE III. Experimental and theoretical $2\,^3P_J$ fine-structure splittings, in MHz.

Interval	This work	Clarke *et al.* [20]	Riis *et al.* [11]	Pachucki and Yerokhin [3]
$2\,^3P_{1-2}$	$62679.247 \pm 0.065(\text{stat.}) \pm 0.023(\text{syst.})$	62679.46(98)	62678.41(65)	62679.318(34)
$2\,^3P_{0-1}$	$155704.499 \pm 0.065(\text{stat.}) \pm 0.087(\text{syst.})$		155704.27(66)	155704.584(48)

[1] Z.-C. Yan and G. W. F. Drake, Phys. Rev. Lett. **74**, 4791 (1995).

[2] K. Pachucki, V. A. Yerokhin, and P. Cancio Pastor, Phys. Rev. A **85**, 042517 (2012).

[3] K. Pachucki and V. A. Yerokhin, Phys. Rev. Lett. **104**, 070403 (2010).

[4] X. Zheng, Y. R. Sun, J.-J. Chen, W. Jiang, K. Pachucki, and S.-M. Hu, Phys. Rev. Lett. **118**, 063001 (2017).

[5] K. Kato, T. D. G. Skinner, and E. A. Hessels, Phys. Rev. Lett. **121**, 143002 (2018).

[6] P. Cancio Pastor, L. Consolino, G. Giusfredi, P. De Natale, M. Inguscio, V. A. Yerokhin, and K. Pachucki, Phys. Rev. Lett. **108**, 143001 (2012).

[7] D. Shiner, R. Dixson, and V. Vedantham, Phys. Rev. Lett. **74**, 3553 (1995).

[8] R. Van Rooij, J. S. Borbely, J. Simonet, M. Hoogerland, K. Eikema, R. Rozendaal, and W. Vassen, Science **333**, 196 (2011).

[9] R. P. M. J. W. Notermans, R. J. Rengelink, and W. Vassen, Phys. Rev. Lett. **117**, 213001 (2016).

[10] Z.-T. Lu, P. Mueller, G. W. F. Drake, W. Nörtershäuser, S. C. Pieper, and Z.-C. Yan, Rev. Mod. Phys. **85**, 1383 (2013).

[11] E. Riis, A. G. Sinclair, O. Poulsen, G. W. F. Drake, W. R. C. Rowley, and A. P. Levick, Phys. Rev. A **49**, 207 (1994).

[12] V. A. Yerokhin, Phys. Rev. A **78**, 012513 (2008).

[13] H. Schüler, Naturwissenschaften **12**, 579 (1924).

[14] H. G. Berry and J. L. Subtil, Phys. Rev. Lett. **27**, 1103 (1971).

[15] B. Fan, A. Lurio, and D. Grischkowsky, Phys. Rev. Lett. **41**, 1460 (1978).

[16] U. Kötz, J. Kowalski, R. Neumann, S. Noehte, H. Suhr, K. Winkler, and G. zu Putlitz, Z. Phys. A: At. Nucl. **300**, 25 (1981).

[17] J. Kowalski, R. Neumann, S. Noehte, K. Scheffzek, H. Suhr, and G. z. Putlitz, Hyperfine Interact. **15**, 159 (1983).

[18] R. Bayer, J. Kowalski, R. Neumann, S. Noehte, H. Suhr, K. Winkler, and G. zu Putlitz, Z. Phys. A: At. Nucl. **292**, 329 (1979).

[19] H. Rong, S. Grafström, J. Kowalski, G. Zu Putlitz, W. Jastrzebski, and R. Neumann, Z. Phys. D: At., Mol. Clusters **25**, 337 (1993).

[20] J. J. Clarke and W. A. van Wijngaarden, Phys. Rev. A **67**, 012506 (2003).

[21] W. A. van Wijngaarden and B. Jian, Eur. Phys. J. Spec. Top. **222**, 2057 (2013).

[22] J. J. Clarke, Ph.D. thesis, York University, 2002.

[23] S. Chen, S. Liang, W. Sun, Y. Huang, H. Guan, and K. Gao, Rev. Sci. Instrum. **90**, 043112 (2019).

[24] Y. Qian, S. Liang, Y. Huang, H. Guan, and K. Gao, Chin. J. Laser **46**, 0211004 (2019).

[25] S. Reinhardt, G. Saathoff, H. Buhr, L. Carlson, A. Wolf, D. Schwalm, S. Karpuk, C. Novotny, G. Huber, M. Zimmermann, R. Holzwarth, T. Udem, T. Hänsch, and G. Gwinner, Nat. Phys. **3**, 861 (2007).

[26] M. Artoni, I. Carusotto, and F. Minardi, Phys. Rev. A **62**, 023402 (2000).

[27] A. Beyer, L. Maisenbacher, A. Matveev, R. Pohl, K. Khabarova, A. Grinin, T. Lamour, D. C. Yost, T. W. Hänsch, N. Kolachevsky *et al.*, Science **358**, 79 (2017).

[28] N. Stone, At. Data Nucl. Data Tables **111–112**, 1 (2016).

[29] X.-Q. Qi, P.-P. Zhang, Z.-C. Yan, G. W. F. Drake, Z.-X. Zhong, T.-Y. Shi, S.-L. Chen, Y. Huang, H. Guan, and K.-L. Gao, arXiv:2009.03114.